

Exotic vs. conventional scaling and universality in a disordered bilayer quantum Heisenberg antiferromagnet

Rastko Sknepnek,¹ Thomas Vojta,¹ and Matthias Vojta²

¹*Physics Department, University of Missouri - Rolla, Rolla, MO 65409*

²*Institut für Theorie der Kondensierten Materie, Universität Karlsruhe, 76128 Karlsruhe, Germany*

(Dated: December 2, 2024)

We present large-scale Monte-Carlo simulations of a two-dimensional (2d) bilayer quantum Heisenberg antiferromagnet with random dimer dilution. In contrast to the exotic scaling scenarios found in many other random quantum systems, the quantum phase transition in this system is characterized by a finite-disorder fixed point with power-law scaling. After accounting for strong corrections to scaling, characterized by a leading irrelevant exponent of $\omega \approx 0.48$, we find universal, i.e., disorder-independent, critical exponents $z = 1.310(6)$ and $\nu = 1.16(3)$. We discuss the consequences of these findings and suggest new experiments.

Quantum phase transitions (QPT) under the influence of quenched disorder are a topic of great current interest. Experimental examples range from localized [1] and itinerant [2] quantum magnets to heavy-fermion compounds [3], high-temperature superconductors [4], metal-insulator [5], as well as superconductor-insulator transitions [6]. These systems display rich new physics but many are still poorly understood. In the context of classical phase transitions, the interplay between disorder and critical fluctuations has a long history. Harris [7] derived a criterion for the stability of a critical point against disorder: If the correlation length exponent ν fulfills the inequality $\nu > 2/d$, where d is the spatial dimensionality, the critical behavior is not influenced by weak disorder. If a clean critical point violates the Harris criterion, the generic result of introducing disorder is a new (finite-disorder) critical point with power-law scaling and new critical exponents which fulfill the Harris criterion [8].

At QPTs, order-parameter fluctuations in space and time have to be considered. Quenched disorder is time-independent, i.e., perfectly correlated in time direction. As a result, disorder effects at QPTs are generically stronger than at classical transitions. Prominent consequences are the infinite-randomness critical points in 1d random spin chains [9] and in 1d [10] and 2d [11] random quantum Ising models. At these infinite-randomness critical points, the dynamical scaling is activated, i.e., the relation between the correlation time ξ_τ and the correlation length ξ is exponential: $\ln \xi_\tau \sim \xi^\mu$. (At a conventional critical point, this relation is a power law, $\xi_\tau \sim \xi^z$). In itinerant electrons systems, the effects of impurities can be even more dramatic. For Ising symmetry, the interplay of quenched disorder and Landau damping of the order parameter fluctuations completely destroys the sharp QPT by smearing [12]. Further unconventional phenomena include non-universal, continuously varying critical exponents, observed in the Griffiths region associated with a QPT [10, 11, 13] or at certain impurity QPTs [14]. These results lead to a general belief that all QPTs in presence of disorder are unconventional.

In this Letter we show that this belief is mistaken. Specifically, we demonstrate that a dimer-diluted 2d spin-1/2 bilayer quantum Heisenberg antiferromagnet has a conventional quantum critical point with power-law scaling. Moreover, the critical exponents are *universal*, i.e., dilution-independent, but only after accounting for corrections to scaling characterized by an irrelevant exponent $\omega \approx 0.48$. The asymptotic dynamical and correlation length exponents are $z = 1.310(6)$ and $\nu = 1.16(3)$ (fulfilling the Harris criterion $\nu > 2/d = 1$ [7, 8]).

Our starting point is the spin-1/2 bilayer quantum Heisenberg antiferromagnet, as depicted in the inset of Fig. 1. The spins in each square-lattice plane interact via exchange J_{\parallel} , and the interplane coupling is J_{\perp} . The clean version of this model has been studied extensively in the past [15, 16]. For $J_{\perp} \gg J_{\parallel}$, neighboring spins from the two layers form singlets, and the ground state is paramagnetic. In contrast, for $J_{\parallel} \gg J_{\perp}$ the system develops Néel order. Both phases are separated by a QPT at $J_{\perp}/J_{\parallel} \approx 2.525$. Importantly, the Berry phase contributions from the two spins of each unit cell exactly cancel, and the continuum limit of this model is an ideal realization of the (2+1)-dimensional O(3) non-linear sigma model without Berry phases [19, 20].

Random disorder is now introduced by removing *pairs* (dimers) of adjacent spins, one from each layer. This type of disorder does *not* introduce random Berry phases, which are present in many other diluted spin systems. Here, by removing dimers, the compensation of Berry phases from adjacent sites is not disrupted by the disorder, and thus this complication is absent. The Hamiltonian of the model with dimer dilution is:

$$H = J_{\parallel} \sum_{\langle i,j \rangle, a=1,2} \epsilon_i \epsilon_j \hat{\mathbf{S}}_{i,a} \cdot \hat{\mathbf{S}}_{j,a} + J_{\perp} \sum_i \epsilon_i \hat{\mathbf{S}}_{i,1} \cdot \hat{\mathbf{S}}_{i,2}, \quad (1)$$

and $\epsilon_i = 0$ ($\epsilon_i = 1$) with probability p ($1 - p$). The phase diagram of the dimer-diluted bilayer Heisenberg model has been studied by Sandvik [17] and Vajk and Greven [18], see Fig. 1. For small J_{\perp} magnetic order survives up to the percolation threshold $p_p \approx 0.4072$,

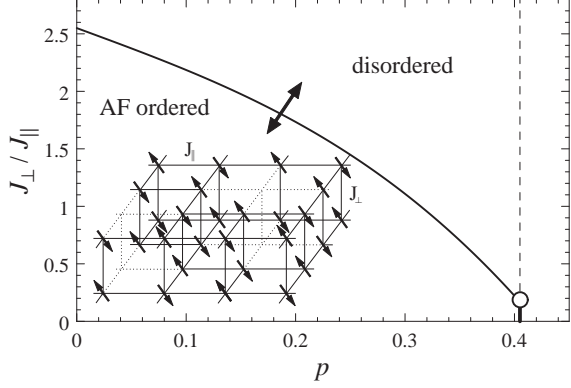


FIG. 1: Phase diagram [18] of the diluted bilayer Heisenberg antiferromagnet, as function of J_{\perp}/J_{\parallel} and dilution p . The dashed line is the percolation threshold, the open dot is the multicritical point of Refs. [17, 18]. The arrow indicates the QPT studied here. Inset: The model: Quantum spins (arrows) reside on the two parallel square lattices. The spins in each plane interact with the coupling strength J_{\parallel} . Interplane coupling is J_{\perp} . Dilution is done by removing dimers.

and a multicritical point exists at $p = p_p$ and $J_{\perp}/J_{\parallel} \approx 0.16$. Here we focus on the generic transition at $0 < p < p_p$, driven by J_{\perp} , where the results of Refs. [17, 18] are inconclusive.

As an aside, we note that site dilution (in contrast to dimer dilution) completely changes the physics for $J_{\perp} \gg J_{\parallel}$. The random Berry phases (which have no classical analogue [20]) are equivalent to impurity-induced moments [21], and those become weakly coupled via bulk excitations. Thus, for all $p < p_p$ the ground state of the system shows long-range order, independent of J_{\perp}/J_{\parallel} !

In order to determine the critical behavior at the QPT most effectively, we simulate a 3d classical Heisenberg model which is in the same universality class as the (2+1)-dimensional O(3) non-linear sigma model discussed above. The disorder is introduced via site dilution perfectly correlated in the imaginary time direction, i.e. the impurities are 1d holes “drilled” through the system. The classical Hamiltonian reads:

$$H = K \sum_{\langle i,j \rangle, \tau} \epsilon_i \epsilon_j \mathbf{S}_{i,\tau} \cdot \mathbf{S}_{j,\tau} + K \sum_{i,\tau} \epsilon_i \mathbf{S}_{i,\tau} \cdot \mathbf{S}_{i,\tau+1}, \quad (2)$$

where $\mathbf{S}_{i,\tau}$ is an O(3) unit vector. The coupling constant K of the classical model, or more precisely, βK is related to the ratio J_{\parallel}/J_{\perp} of the quantum model. Here, $\beta \equiv 1/T$ where T is an effective “classical” temperature, not equal to the real temperature which is zero. In our simulations we set $K = 1$ and drive the classical system through the transition by tuning the classical temperature T .

We determine the critical behavior of the classical model (2) by performing Monte-Carlo simulations using the highly efficient Wolff cluster algorithm [22, 23]. We study linear sizes up to $L = 120$ in space direction and

$L_{\tau} = 384$ in imaginary time direction for four impurity concentrations $p = \frac{1}{8}, \frac{1}{5}, \frac{2}{7}$ and $\frac{1}{3}$. The results are averaged over a large number of disorder realizations ranging from 10^4 for the smallest systems to 1000 for the largest. Each sample is equilibrated using 100 Monte-Carlo sweeps (spin-flips per site). For large dilutions, $p = \frac{2}{7}$ and $\frac{1}{3}$ we perform both Wolff and Metropolis sweeps to equilibrate small dangling clusters. During the measurement period of another 100-200 sweeps we calculate the magnetization, susceptibility, specific heat and correlation functions.

A quantity particularly suitable to locate the critical point and to extract high precision values for the exponents z and ν is the Binder ratio:

$$g_{av} = \left[1 - \frac{\langle |\mathbf{M}|^4 \rangle}{3 \langle |\mathbf{M}|^2 \rangle^2} \right]_{av}, \quad (3)$$

where $\mathbf{M} = \sum_{i,\tau} \mathbf{S}_{i,\tau}$, $[\dots]_{av}$ denotes the disorder average and $\langle \dots \rangle$ denotes the Monte-Carlo average for each sample. This quantity has scale dimension 0. Thus, its finite-size scaling form is given by

$$g_{av} = \tilde{g}_C(tL^{1/\nu}, L_{\tau}/L^z) \quad \text{or} \quad (4)$$

$$g_{av} = \tilde{g}_A(tL^{1/\nu}, \log(L_{\tau})/L^{\mu}) \quad (5)$$

for conventional scaling or for activated scaling, respectively. Two important characteristics immediately follow: (i) For fixed L , g_{av} has a peak as a function of L_{τ} . The position L_{τ}^{\max} of the peak marks the *optimal* sample shape, where the ratio L_{τ}/L roughly behaves like the corresponding ratio of the correlation lengths in time and space directions, ξ_{τ}/ξ . At the critical point, the peak value g_{av}^{\max} is independent of L . Thus, for power law scaling, plotting g_{av} at the critical temperature vs. L_{τ}/L_{τ}^{\max} should collapse the data, without the need for a value of z . In contrast, for activated scaling the g_{av} data should collapse when plotted as a function of $\log(L_{\tau})/\log(L_{\tau}^{\max})$. (ii) For samples of the optimal shape ($L_{\tau} = L_{\tau}^{\max}$), plots of g_{av} vs. temperature for different L cross at the critical temperature T_c . Based on these two characteristics, we use a simple iterative procedure to determine both the optimal shapes and the location of the critical point.

We now turn to the results of our Monte-Carlo simulations. In order to distinguish between activated and power-law dynamical scaling we perform a series of calculations at the critical temperature. The upper panel of Fig. 2 shows the Binder ratio g_{av} as a function of L_{τ} for various $L = 5 \dots 100$ and dilution $p = \frac{1}{5}$ at $T = T_c = 1.1955$. The statistical error of g_{av} is below 0.1% for the smaller sizes and not more than 0.2% for the largest systems. As expected at T_c , the maximum Binder ratio for each of the curves does not depend on L . To test the conventional power-law scaling form, eq. (4), we plot g_{av}/g_{av}^{\max} as a function of L_{τ}/L_{τ}^{\max} in the lower panel of Fig. 2. The data scale extremely well, giving statistical errors of L_{τ}^{\max} in the range between 0.3% and 1%. For

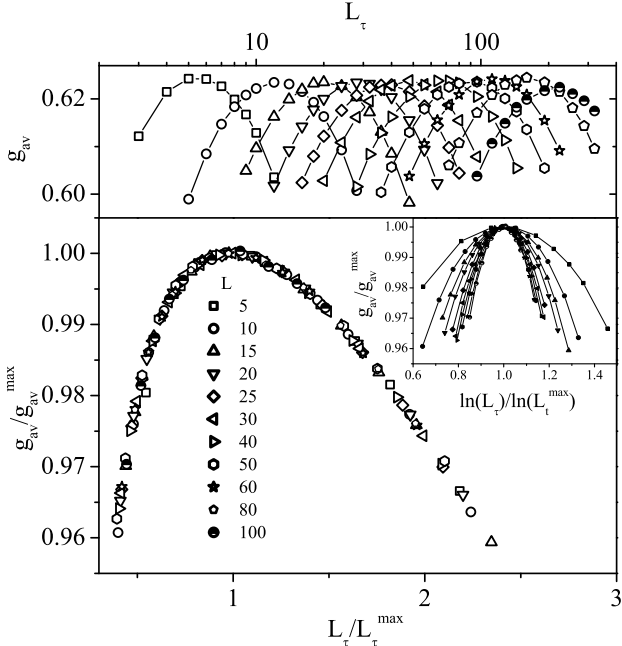


FIG. 2: Upper panel: Binder ratio g_{av} as a function of L_{τ} for various L ($p = \frac{1}{5}$). Lower panel: Power-law scaling plot g_{av}/g_{av}^{max} vs. L_{τ}/L_{τ}^{max} Inset: Activated scaling plot g_{av}/g_{av}^{max} vs. $\log(L_{\tau})/\log(L_{\tau}^{max})$.

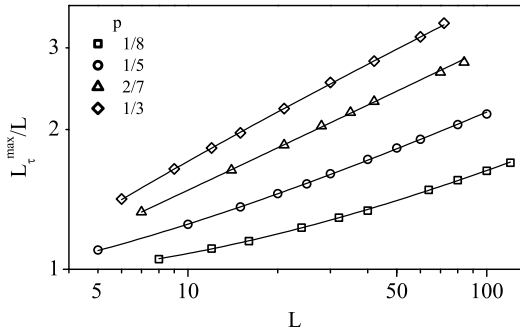


FIG. 3: L_{τ}^{max}/L vs. L for four disorder concentrations $p = \frac{1}{8}, \frac{1}{5}, \frac{2}{7}$ and $\frac{1}{3}$. Solid lines: Fit to $L_{\tau}^{max} = aL^z(1 + bL^{-\omega_1})$ with $z = 1.310(6)$ and $\omega_1 = 0.48(3)$.

comparison, the inset shows a plot of g_{av} as a function of $\log(L_{\tau})/\log(L_{\tau}^{max})$ corresponding eq. (5). The data clearly do not scale which rules out the activated scaling scenario. The results for the other three impurity concentrations $p = \frac{1}{8}, \frac{2}{7}, \frac{1}{3}$ are completely analogous.

Having established that the dynamical scaling is of conventional power-law type we proceed to determine the dynamical exponent z . In Fig. 3, we plot L_{τ}^{max} vs. L for all four dilutions p . The curves show significant deviations from pure power-law behavior. These deviations can be attributed to corrections to scaling, produced by one or more irrelevant operators. In such a situation, a direct power-law fit of the data will only yield *effective* exponents. To determine the true *asymptotic* exponents

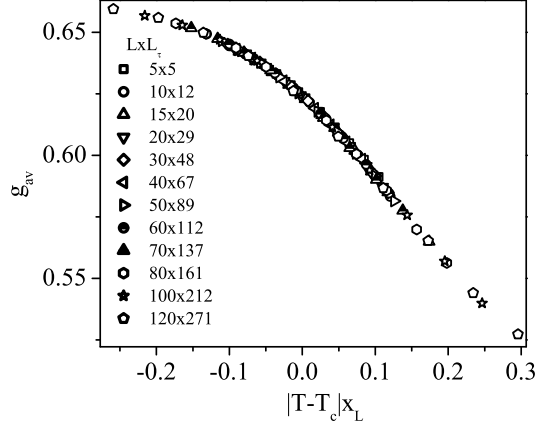


FIG. 4: Scaling plot of g_{av} vs. $(T - T_c)x_L$ for $p = 0.2$.

we take the leading correction to scaling into account, i.e., we use the ansatz $L_{\tau}^{max}(L) = aL^z(1 + bL^{-\omega_1})$ with universal (dilution-independent) exponents z and ω_1 but dilution-dependent a and b . A combined fit of all four curves gives $z = 1.310(6)$ and $\omega_1 = 0.48(3)$ where the number in brackets is the standard deviation of the last given digit. The quality of the fit is very high ($\chi^2 \approx 0.7$), and it is also robust against removing complete data sets or removing different points from the lower or upper end of each set. We thus conclude that the asymptotic dynamical exponent z is indeed universal. (Note that the leading corrections to scaling vanish very close to $p = \frac{2}{7}$; the curvature of the $L_{\tau}^{max}(L)$ curves in Fig. 3 is opposite above and below this concentration.)

To determine the correlation length exponent ν , we perform simulations in the vicinity of T_c for samples with the optimal shape ($L_{\tau} = L_{\tau}^{max}$) to keep the second argument of the scaling function (4) constant. Fig. 4 shows a scaling plot of g_{av} vs. $x_L(T - T_c)$ for impurity concentration $p = \frac{1}{5}$. Again, the data scale very well, but since the scaling function lacks the characteristic maximum, the error of the resulting scaling factor x_L is somewhat larger (1...2%) than that of L_{τ}^{max} . The same quality of scaling was achieved for the other impurity concentrations. In Fig. 5, we plot the scaling factor x_L vs. L for all four data sets. We use the ansatz $x_L = cL^{1/\nu}(1 + dL^{-\omega_2})$ to extract the asymptotic ν and the leading corrections to scaling. Here ν and ω_2 are universal. A combined fit of all four curves gives $\nu = 1.16(3)$ and $\omega_2 = 0.5(1)$. As above, the fit is robust and of high quality ($\chi^2 \approx 1.2$). Importantly, as expected for the true asymptotic exponent, ν fulfills the Harris criterion [7], $\nu > 2/d=1$. We also note that both irrelevant exponents ω_1 and ω_2 agree within their error bars, suggesting that the same irrelevant operator controls the leading corrections to scaling for both z and ν .

We have also calculated the exponents β and γ . However, the corrections to scaling for magnetization and susceptibility are even stronger than that of the Binder ra-

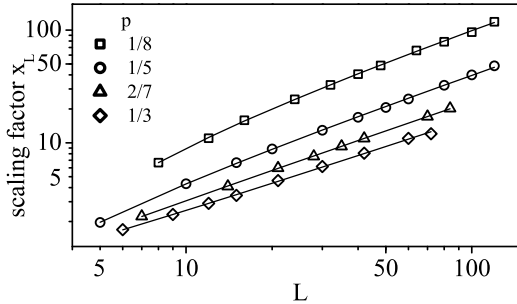


FIG. 5: Scaling factor vs. L for four disorder concentrations $p = \frac{1}{8}, \frac{1}{5}, \frac{2}{7}$ and $\frac{1}{3}$. Solid lines: Fit to $x_L = cL^{1/\nu}(1 + dL^{-\omega_2})$ with $\nu = 1.16(3)$ and $\omega_2 = 0.5(1)$.

tio, leading to larger errors for β and γ . We have found $\beta/\nu = 0.56(5)$ and $\gamma/\nu = 2.15(10)$. These exponents fulfill the hyperscaling relation $2\beta + \gamma = (d + z)\nu$ which is another argument for our results being asymptotic rather than effective exponents.

In summary, we have performed Monte-Carlo simulations of a 3d classical Heisenberg model with linear impurities which is in the same universality class as the dimer-diluted bilayer quantum Heisenberg antiferromagnet. The QPT in this system is characterized by a conventional, finite-disorder critical point with power-law scaling, in contrast to the wide-spread belief that all QPTs in the presence of disorder are exotic. (Note that the Ising version of our model, the diluted 2d random transverse Ising model, shows an infinite-randomness critical point [11, 25].) Moreover, the asymptotic critical exponents are universal, i.e., dilution-independent.

Let us briefly compare our findings to previous work. The multicritical point at $p = p_p$ and $J_\perp/J_\parallel \approx 0.16$, identified in Refs. [17, 18], has a dynamical exponent $z \approx 1.3$. Within the error bars, this value coincides with the one found here for the generic $p < p_p$ transition. We see no a-priori reason for this coincidence, so far it is unclear whether or not it is accidental. Vajk and Greven [18] also quote exponent values for $p < p_c$. At dilution $p = 0.25$ they find $z = 1.07$ and $\nu = 0.89$, different from our results. However, as the authors of Ref. [18] point out, a value of $\nu < 1$ violates the Harris criterion, indicating that it represents an effective rather than an asymptotic exponent. It would also be useful to compare our findings with analytical results. To the best of our knowledge, the only quantitative result is a resummation of the 2-loop ϵ -expansion [24]. The predicted critical exponents significantly differ from ours. However, they also violate the Harris criterion, casting doubt on their validity.

Finally, we comment on experiments. If chemical doping replaces magnetic by non-magnetic ions in a 2d anti-ferromagnet, e.g., Cu by Zn in $\text{YBa}_2\text{Cu}_3\text{O}_6$, the case of site rather than dimer dilution is realized. The most promising way to effectively achieve bond dilution is the introduction of strong antiferromagnetic inter-dimer

bonds at random locations. Thus we propose to study magnetic transitions in bond-disordered systems; those transitions can be expected to be in the same universality class as the one studied here. One candidate material – albeit 3d – is $(\text{Ti},\text{K})\text{CuCl}_3$ under pressure; interesting quasi-2d compounds are $\text{SrCu}_2(\text{BO}_3)_2$ or $\text{BaCuSi}_2\text{O}_6$, where suitable dopants remain to be found.

We acknowledge support from the University of Missouri Research Board and from the DFG Center for Functional Nanostructures Karlsruhe.

- [1] W. Wu *et al.*, Phys. Rev. Lett. **67**, 2076 (1991).
- [2] J. DiTusa *et al.*, cond-mat/0306541.
- [3] C. L. Seaman *et al.*, Phys. Rev. Lett. **67**, 2882 (1991); B. Andranka and A. M. Tsvelik, Phys. Rev. Lett. **67**, 2886 (1991); M. C. de Andrade *et al.*, Phys. Rev. Lett. **81**, 5620 (1998).
- [4] C. Panagopoulos *et al.*, Phys. Rev. B **66**, 064501 (2002).
- [5] S. V. Kravchenko *et al.*, Phys. Rev. B **51** 7038 (1995); E. Abrahams, S. Kravchenko, and M. Sarachik, Rev. Mod. Phys. **73**, 251 (2001).
- [6] A. F. Hebard and M. A. Paalanen, Phys. Rev. Lett. **65**, 927 (1990).
- [7] A. B. Harris, J. Phys. C **7**, 1671 (1974).
- [8] J. Chayes *et al.*, Phys. Rev. Lett. **57**, 2999 (1986).
- [9] S. K. Ma, C. Dasgupta, and C.-K. Hu, Phys. Rev. Lett. **43**, 1434 (1979); R. N. Bhatt and P. A. Lee, *ibid.* **48**, 344 (1982); D. S. Fisher, Phys. Rev. B **50**, 3799 (1994).
- [10] D. S. Fisher, Phys. Rev. Lett. **69**, 534 (1992); Phys. Rev. B **51**, 6411 (1995); A. P. Young and H. Rieger, *ibid.* **53**, 8486 (1996);
- [11] C. Pich *et al.*, Phys. Rev. Lett. **81**, 5916 (1998); O. Motrunich *et al.*, Phys. Rev. B **61**, 1160 (2000).
- [12] T. Vojta, Phys. Rev. Lett. **90**, 107202 (2003).
- [13] R. B. Griffiths, Phys. Rev. Lett. **23**, 17 (1969); B. M. McCoy, Phys. Rev. Lett. **23**, 383 (1969).
- [14] A. Georges and A. M. Sengupta, Phys. Rev. Lett. **74**, 2808 (1995), and references therein.
- [15] K. Hida, J. Phys. Soc. Jpn. **59**, 2230 (1990); A. J. Millis and H. Monien, Phys. Rev. Lett. **70**, 2810 (1993).
- [16] A. W. Sandvik and D. J. Scalapino, Phys. Rev. Lett. **72**, 2777 (1994); P. V. Shevchenko, A. W. Sandvik and O. P. Sushkov, Phys. Rev. B **61**, 3475 (2000).
- [17] A. W. Sandvik, Phys. Rev. Lett. **89**, 177201 (2002).
- [18] O. P. Vajk and M. Greven, Phys. Rev. Lett. **89**, 177202 (2002).
- [19] S. Chakravarty, B. I. Halperin and D. R. Nelson, Phys. Rev. B **39**, 2344 (1989).
- [20] S. Sachdev, *Quantum Phase Transitions*, Cambridge University Press, Cambridge (1999).
- [21] S. Sachdev and M. Vojta, in Proceedings of the XIII International Congress on Mathematical Physics, eds. A. Fokas *et al.*, International Press, Boston (2001).
- [22] U. Wolff, Phys. Rev. Lett. **62**, 361 (1989).
- [23] Since the classical model is not frustrated, we can use cluster algorithms to reduce critical slowing down.
- [24] V. Blavats'ka, C. von Ferber, and Yu. Holovatch, Phys. Rev. B **67**, 094404 (2003).
- [25] T. Senthil and S. Sachdev, Phys. Rev. Lett. **77**, 5292 (1996).